LETTERS
PUBLISHED ONLINE: 30 OCTOBER 2011 | DOI: 10.1038/NMAT3148
nature materials

Optical negative refraction by four-wave mixing in thin metallic nanostructures

Stefano Palomba[1], Shuang Zhang[1,2], Yongshik Park[1], Guy Bartal[1,3], Xiaobo Yin[1,4] and Xiang Zhang[1,4]*

The law of refraction first derived by Snellius and later introduced as the Huygens–Fermat principle[1], states that the incidence and refracted angles of a light wave at the interface of two different materials are related to the ratio of the refractive indices in each medium. Whereas all natural materials have a positive refractive index and therefore exhibit refraction in the positive direction, artificially engineered negative index metamaterials have been shown capable of bending light waves negatively[2–8]. Such a negative refractive index is the key to achieving a perfect lens that is capable of imaging well below the diffraction limit[9–11]. However, negative index metamaterials are typically lossy, narrow band, and require complicated fabrication processes. Recently, an alternative approach to obtain negative refraction from a very thin nonlinear film has been proposed[12,13] and experimentally demonstrated in the microwave region[14–16]. However, such approaches use phase conjugation, which makes optical implementations difficult. Here, we report a simple but different scheme to demonstrate experimentally nonlinear negative refraction at optical frequencies using four-wave mixing in nanostructured metal films. The refractive index can be designed at will by simply tuning the wavelengths of the interacting waves, which could have potential impact on many important applications, such as superlens imaging.

Snell's law can be generalized to nonlinear processes by taking into account not only the different direction of the refracted electromagnetic (EM) wavevector but also the frequency at which it is emitted[17]. Frequency mixing of EM fields in a nonlinear medium requires phase matching to obtain efficient optical frequency conversion[18,19], namely, the nonlinear response of every atom in the material has to sum up constructively. In dielectric materials, the nonlinear susceptibility is typically weak, hence an efficient phase matching process requires a bulk material much larger than the wavelength. In metals, on the other hand, the nonlinear interaction can be very strong, such that even a deep-subwavelength thick metal film can exhibit significant nonlinearities[18,20]. When the metal thickness is less than its skin depth, the nonlinear interaction, although not benefiting from full phase matching (momentum conservation in all directions), presents an additional degree of freedom as the newly generated wave can now emerge in both forward and backward directions (Fig. 1). Moreover, the high intrinsic nonlinearities of metals can be further enhanced by nanostructuring the surface[21,22] such that even the partial phase matching along the interface can result in a moderate nonlinear efficiency.

In this Letter, we experimentally demonstrate nonlinear optical negative refraction in thin metallic nanostructures. We use a degenerate four-wave mixing (4WM) process to show efficient frequency conversion by a 20 nm thick gold film where a wave at the newly generated frequency emerges at a negative angle relative to the exciting wave. The ratio between the sines of the incidence and nonlinearly refracted angles remains a negative constant and depends only on the wavelength ratio, which therefore rigorously fulfils Snell's law, extending the phenomenon of negative refraction into the nonlinear regime. Furthermore, we use a metamaterial constructed from $Au/SiO_2/Au$ nanodisk structures to enhance the nonlinear efficiency by means of localized plasmon resonance[23]. The enhanced nonlinearity gives rise to excellent efficiency in spite of the ultra-small thickness of the nonlinear film, enabling for the first time the realization of optical nonlinear negative refraction, which cannot be obtained in bulk dielectrics because of strict phase matching conditions. We further observed that this nonlinear negative refraction can be realized with evanescent waves. The ability of a very thin slab to generate negative refraction could result in super-resolution imaging in the visible region by converting evanescent waves with high spatial frequency components into propagating waves by means of nonlinear wave mixing processes.

Here, we employ a degenerate 4WM scheme, which is a third order nonlinear process that couples four EM fields where two or more of them are at the same frequency. Such mixing between two plane waves at frequency ω_1 and a third plane wave at ω_2 would result in a new wave at frequency $\omega_3 = 2\omega_1 - \omega_2$. Incident on a thin nonlinear medium, such as gold film, the wave-mixing takes place via the surface nonlinearity[24], where the phase matching condition applies only along the metal–dielectric interface.

$$k_3 = \frac{2\pi}{\lambda_3}\sin\theta_3 = 2\frac{2\pi}{\lambda_1}\sin\theta_1 - \frac{2\pi}{\lambda_2}\sin\theta_2 \qquad (1)$$

Here, k_1, k_2 and k_3 are respectively the wavevectors of the pump beam at frequency ω_1 and incidence angle θ_1, the probe beam at frequency ω_2 and incidence angle θ_2, and the nonlinearly generated, refracted beam at frequency ω_3 and incidence angle θ_3. The λ_i are the wavelengths in the media for the different frequencies. Figure 1a describes the general case of in-plane phase matching where the pump field and the probe field impinge on the nonlinear film at arbitrary incidence angles. The nonlinear process in the thin film gives rise to two beams at frequency $\omega_3 = 2\omega_1 - \omega_2$, generated with equal efficiency in the forward and backward directions. The most interesting scenario occurs when the pump beam incidence angle is set to zero, that is $\theta_1 = 0$, and the phase matching condition can be rewritten as

$$\frac{2\pi}{\lambda_3}\sin\theta_3 = -\frac{2\pi}{\lambda_2}\sin\theta_2$$

resulting in a new wave at ω_3 generated by nonlinear polarization that refracts at a negative angle with respect to the incidence angle of the probe beam, as illustrated in Fig. 1b. Interestingly, the relation

[1]NSF Nano-scale Science and Engineering Center (NSEC), 3112 Etcheverry Hall, University of California, Berkeley, California 94720, USA, [2]Department of Physics and Astronomy, University of Birmingham, Birmingham B15 2TT, UK, [3]Department of Electrical Engineering, Technion, 32000 Haifa, Israel, [4]Material Sciences Division, Lawrence Berkeley National Laboratory, Berkeley, California 94720, USA. *e-mail: xiang@berkeley.edu.

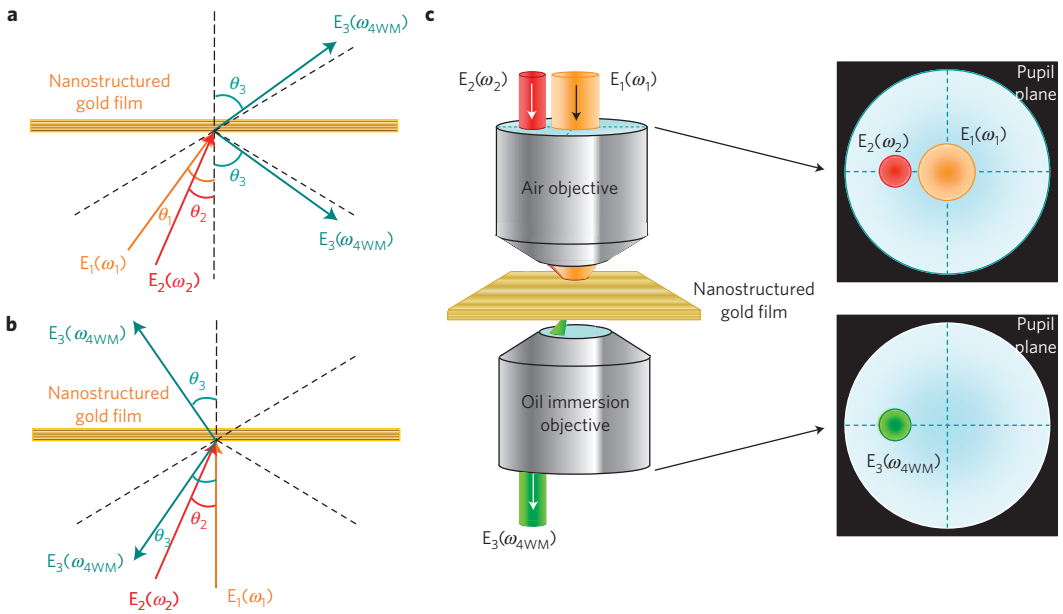

Figure 1 | Schematics of the degenerate 4WM process on a thin nonlinear film. a, The general case with arbitrary incidence angles of the pump (ω_1) and probe (ω_2) beams. The directions of the forward and backward 4WM waves are determined by the in-plane phase matching condition. **b**, The special case with normal incidence ($\theta_1 = 0$) of the pump beam. The forward nonlinear 4WM beam exhibits negative refraction relative to the probe beam. The ratio between the sines of the incident probe beam angle and the refracted angle of the 4WM wave is a constant that depends only on the ratio of the two wavelengths. **c**, Schematic illustration of the experimental set-up. Two objectives with large back apertures are confocally aligned and serve as Fourier transform lenses converting the spatial positions of the beams, relative to the back aperture of the lenses, to the propagation directions of the wavevectors in *k*-space, and therefore to the incidence or refracted angles. Both the pump and probe beams are launched through the top air objective at different incidence angles, which can be precisely determined by mapping the partial reflection from the lens. The oil immersion objective collects the nonlinear generated photons at the 4WM frequency in the forward direction. Imaging the pupil plane of the objectives provides a measurement of both the refracted and incidence angles with an accuracy limited only by the ratio between the physical size of the actual beam and the diameters of the back aperture of the objective. Furthermore, the beam with the smallest physical size determines the area of nonlinear interaction, and hence impacts the image quality because of the increased divergence in wavevector for a small sized illumination beam.

between the incidence and refracted angles strictly obeys Snell's law, where the ratio between the incident and refracted wavelengths plays the role of the refractive index,

$$\frac{\sin\theta_3}{\sin\theta_2} = -\frac{\lambda_3}{\lambda_2}$$

Thus, the thin metallic film acts as an interface between two media with opposite signs of refractive index, where the refraction process is extended to the nonlinear regime. The ratio between the sines of the incidence and refracted angles is a constant that depends only on the wavelengths in the respective media.

This nonlinear negative refraction is experimentally demonstrated using a thin gold film atop a glass substrate; the experimental set-up is illustrated in Fig. 1c. We use two confocal objectives to image the Fourier plane onto CCD cameras such that the propagation directions of the wavevectors in *k*-space are mapped into the physical space. A pulsed Ti:Sapphire laser with 130 fs pulses at a wavelength $\lambda_1 = 775$ nm is used as the pump beam. To show the dependence of the refracted angle on the interacting beam wavelengths, measurements are carried out using probe beams at two different wavelengths (1,135 nm and 1,240 nm) generated by an optical parameter oscillator. The results are shown in Fig. 2, where the pupil plane images at various incidence angles are shown. The probe incidence angles are 0 and 22.3° in the *y*-direction, and 23.2° in the *x*-direction, shown in Fig. 2a,c and e, respectively, while the pump beam is set to normal incidence to fulfil the requirement for the nonlinear Snell's law. The generated 4WM signals ($\lambda_3 = 563$ nm), shown in Fig. 2b,d and f respectively, clearly exhibit negative refraction, being located on the same side of the Fourier plane as the probe beam for all incidence angles. Note that, for incidence angles tuned along the *x* and *y* orientations, the polarization states of the probe beams are transverse magnetic (TM) and transverse electric (TE), respectively. Nonetheless, nonlinear negative refraction is observed in both cases, proving that negative refraction is not affected by the polarization state, in stark contrast to most of the negative index metamaterials and photonic crystals demonstrated thus far.

The relations between the sines of the nonlinearly refracted and incident beams, shown in Fig. 3a, prove that Snell's law applies to nonlinear refraction. The measurements are well fitted by straight lines with slopes (or effective nonlinear refractive indices) of −2.7 and −3.3 for probe wavelengths at 1,135 nm and 1,240 nm, respectively. Both measurements closely match the theoretical effective refractive indices of −2.9 and −3.3, given as the ratio between the probe and 4WM wavelengths. This nonlinear approach provides a convenient way to realize the desired negative refraction by merely tuning the wavelength of the pumping beam. More importantly, the phase matching condition along the thin film dictates that Snell's law is rigorously obeyed for all angles, whereas in metamaterials and photonic crystals, Snell's law holds only approximately, owing to the nonlocal effect arising from their finite lattice constants. As a further development of the negative refraction demonstrated using phase conjugation[12,13] and its implementation at microwave frequencies[14–16], the optical 4WM approach demonstrated here does not involve a time reversal process where forward and backward waves have the same frequency and are the exact counter-propagating time replicas of each other. Consequently, the effective index, which is determined by the ratio of the wavelengths of the waves involved in the nonlinear interaction, could be arbitrarily small or large, whereas

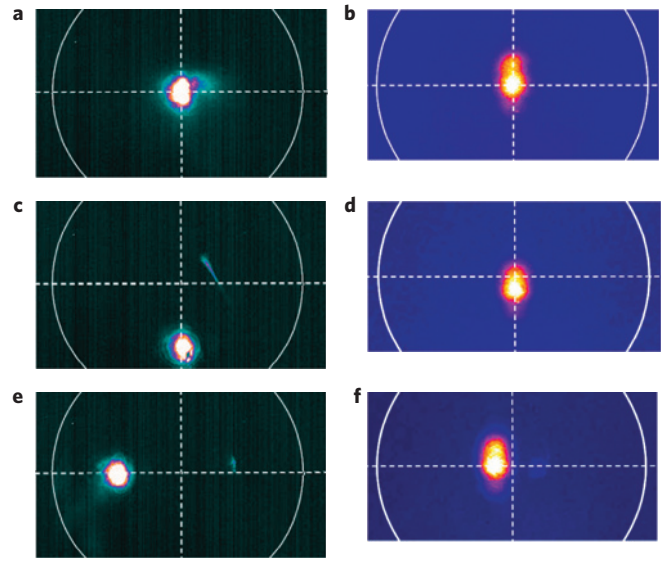

Figure 2 | Fourier plane of the detected signals. a–f, Fourier plane images of the probe beam (**a**,**c**,**e**) and the forward 4WM signal (**b**,**d**,**f**) with a probe beam wavelength of 1,240 nm. The position of the beam is directly related to the sines of the incidence or refracted angles. The incidence angles of the probe beam are $\theta_2 = 0$ (**a**), $\theta_2 \sim 22.3°$ (**c**), $\theta_2 \sim 23.2°$ (**e**), on a 20 nm thick gold film, while the refracted angles of the 4WM beams are $\theta_2 = 0$ (**b**), $\theta_2 \sim 4.9°$ (**d**), $\theta_2 \sim 6.7°$ (**f**), respectively. The positions of both the probe beam and the forward 4WM beam are located on the same side of the pupil plane images, confirming negative refraction of the generated nonlinear wave. The nonlinear refraction depicted here is polarization independent, as evident from the pupil plane images with both TE (**c**,**d**) and TM (**e**,**f**) polarized probe beams, in which the incidence angles are tuned along the vertical and horizontal directions, respectively.

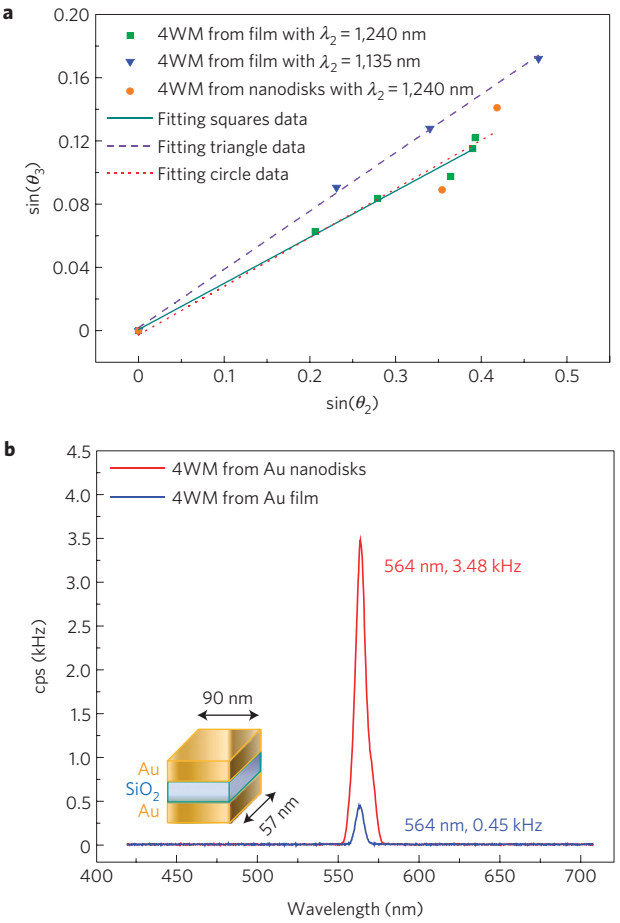

Figure 3 | Four-wave mixing analysis. a, Nonlinear Snell's law of 4WM for thin gold film nanosystems at $\lambda_2 = 1,240$ nm (rectangles) and $\lambda_2 = 1,135$ nm (triangles) and a nanodisk array at $\lambda_2 = 1,240$ nm (circles). The incidence angle of the probe beam, θ_2, and the refracted angle of the 4WM signals, θ_3, strictly obey Snell's law, resulting in a constant ratio between their sines that depends only on the wavelengths. Linear fitting of the measurements shows good agreement with the theoretical results. The position of the probe beam and the 4WM signal are precisely determined by a Gaussian centroid fit algorithm. **b**, The 4WM signal generated from both the thin gold film (blue) and thin film of nanodisks (red). The forward 4WM signal obtained for the nanodisk structures is about ten times stronger than that for the thin gold film owing to the strong field confinement at localized surface plasmon resonances. The inset shows the geometry of the Au/SiO_2/Au nanodisks examined in the experiments. To match the resonance wavelength of the pump beam the nanodisks are designed 57 nm in width and 90 nm in length with a period of 400 nm on a glass substrate. The thicknesses of both gold and SiO_2 layers are 20 nm each.

the phase conjugation approach leads only to a fixed refractive index of −1. Furthermore, because the phase matching condition works for both propagating and evanescent waves with arbitrarily large in-plane wavevectors, the deep subwavelength information contained in the evanescent signal can be transferred to the 4WM waves as they have different frequencies.

Nevertheless, it is necessary to emphasize that super-resolution is relevant only for smooth and homogeneous surfaces. In the case of non-smooth and non-homogeneous surfaces, the in-plane momentum is limited by the dimensions of the surface nanostructures, which must be much smaller than the wavenumbers of the EM wave interacting with the surface. Furthermore, when the in-plane wavevectors are on the same scale as the surface nanostructures, a strong angular dependence is expected as well. Such a capability, and the flexibility to achieve a desired optical negative index at will, may have a significant impact on applications such as super-resolution imaging and nanoscopic metrology.

Although the small thickness of the metal film enables one to access the strong metal nonlinearity, the 4WM process on a thin smooth metal film does not take any advantage of the additional enhancement mechanisms available in metal–dielectric systems. Surface plasmons[25] have been shown to exhibit strong resonances owing to the excitation of the collective motions of conduction electrons, accompanied by a strong enhancement of the local field. As all nonlinear effects increase rapidly with the electric field, such an enhancement can considerably increase the 4WM process for nonlinear negative refraction. Here we apply this plasmonic resonance by engineering a metamaterial based on a nanodisk array structure[23]. The nanodisks consist of a layer of SiO_2 sandwiched between two thin layers of gold, as illustrated in the inset of Fig. 3. In particular, we tailor the nanodisk dimensions to maximize the field confinement at the pump frequency (ω_1), on which the nonlinear polarization depends most strongly.

Similarly to the nonlinear measurement on the metal film, negative refraction is obtained for all the incidence angles and the results, depicted in Fig. 3a, show good agreement with the calculated Snell's law. On the other hand, the nano-engineered disk structures exhibit considerable enhancement of 4WM signals compared with the metal film. The plot in Fig. 3b shows the 4WM signal detected through a 565/20 nm band pass filter, clearly showing about one order of magnitude enhanced 4WM compared with that measured from a smooth 20 nm gold film. We experimentally obtain the efficiency of nonlinear 4WM generation, which is measured and calculated using a reference beam. The efficiency obtained is

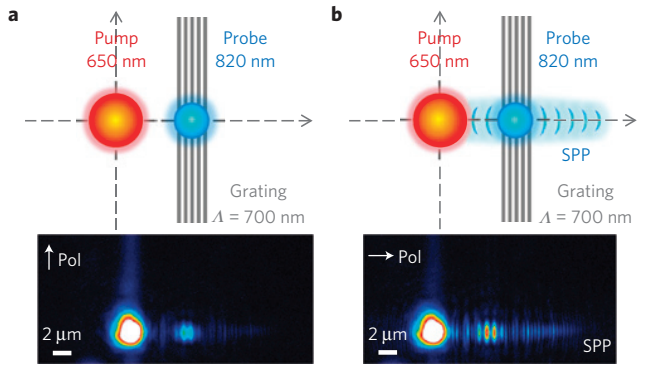

Figure 4 | Top view schematic of the experiment and the corresponding experimental images collected by a CCD positioned at the imaging plane. The real-space images show the position of both the pump and probe beam. **a**, The polarization of the probe beam is set parallel to the grating (*s*-pol) which does not launch any SPP waves. **b**, In contrast, when the polarization of the probe beam is set orthogonal to the grating structure (*p*-pol), then the probe beam can be efficiently coupled to the SPP propagating perpendicular to the grating. In both cases, the pump beam is positioned in the centre of the objective and clearly interacts with the surface wave in the case of the *p*-polarized pump beam.

about $\eta = 9 \times 10^{-8}$ for a 20 nm continuous gold film, which is significantly stronger than any other conventional nonlinear optical materials of the same thickness[22]. Furthermore, the capability of metamaterials to tailor their nonlinear response is demonstrated by the considerably increased efficiency of $\eta = 10^{-6}$ measured in the nanodisk metamaterial.

As a matter of fact, the phase matching condition (equation (1)) at the interface remains valid not only for the propagating waves but also for the evanescent components. Indeed, when one of the probe beams is a surface wave with a wavevector of k_{spp} larger than the wavevectors of the propagating waves, the 4WM phase matching condition may result in negatively refracted propagating fields

$$k_3(\lambda_{4wm})\sin\theta_3 = 2k_1\sin\theta_1 - k_2 = 2k_1\sin\theta_1 - k_{ssp}$$

The high spatial frequency components (evanescent) of a sub-wavelength object can therefore be transferred to a propagating beam that can subsequently be detected and processed by conventional optical imaging in the far-field. This is distinctly different from the phase conjugation scheme, which not only amplifies the evanescent components but also restricts the observation to the near-field. We further demonstrate negative refraction by 4WM involving evanescent waves. A $\Lambda = 700$ nm period metallic grating is fabricated on the surface of a 50 nm thick gold film to launch an evanescent surface plasmon polariton (SPP) probe beam at the gold–air interface. This evanescent wave propagates along the interface and interacts with a pump laser (650 nm) at a location away from the grating, producing a wave mixing beam propagating into the glass substrate. Figure 4a,b shows the schematic top view of the experiment with the corresponding images collected by a CCD camera for both *s* and *p* polarized probe beams, respectively. When the polarization of the probe beam is set parallel to the grating (*s*-polarization), no SPP waves are launched; whereas the *p*-polarized probe beam is efficiently launched perpendicular to the grating (Fig. 4b). When the temporal delay between the pump and probe pulses is zero, momentum and energy conservation are fulfilled and the third order nonlinear susceptibility generates wave mixing. Through the 4WM process of the incident pump beam normal to the surface and the in-plane evanescent SPP wave (k_{spp}), a new beam is observed at the 4WM frequency, acquiring a momentum propagating in the negative refraction direction given by $-k_{spp}$. The

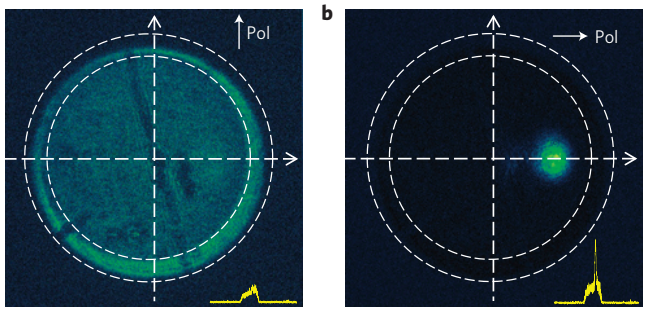

Figure 5 | Fourier plane images of the detected signal. a, Fourier plane image when the probe beam polarization is set parallel to the grating (*s*-pol). With this polarization there is no SPP probe wave and therefore no 4WM is observed either at the Fourier plane or at the spectrometer (inset image). The spectrum shows just a continuum in the detection band of the filter used (500–560 nm). **b**, The polarization of the probe beam is set orthogonal to the grating (*p*-pol), which fulfils the phase matching conditions to launch SPP waves at the air-gold interface. One of these evanescent waves can interact with the pump beam and generate the 4WM, seen as a clear spot at the Fourier plane and as a clear peak at 537 nm, above the continuum. The 4WM spot corresponds to a negative refracted angle of ~27.7°, which agrees well with the theoretical predictions (~26.8°). Note that the position of the 4WM beam is located on the right-hand side of the Fourier plane (the side on which the grating is located).

observed 4WM spot in the *k*-plane agrees well with the theoretical predictions (Fig. 5). This experiment extends the observation of negative refraction by means of 4WM to the regime of the optical near-field, where the involved momentum of evanescent waves can be much larger than their free space counterparts. As surface waves do not suffer radiation losses, nonlinear processes with evanescent waves also improve the wave mixing detection.

We have demonstrated the nonlinear negative refraction of light resulting from a four-wave mixing process in metallic nanostructures. The in-plane phase matching condition leads to Snell's law in its nonlinear form, where the nonlinear effective refractive index depends only on the wavelength ratio of the interacting waves. Nonlinear negative refraction is also possible for evanescent waves. These results show the new potential of using a nonlinear process towards achieving high resolution and background free imaging at the nanoscale. As both the metal film and nanodisk array are not diffraction limited and can accommodate very large wavevectors, the imaging resolution can be increased to provide efficient nonlinear super-resolution imaging and stimulate further investigations of time reversal and negative refraction with nonlinear wave mixing.

Received 7 March 2011; accepted 17 September 2011; published online 30 October 2011

References

1. Huygens, C. *Traité de la Lumiere* (Pieter van der Aa, 1690).
2. Shelby, R. A., Smith, D. R. & Schultz, S. Experimental verification of a negative index of refraction. *Science* **292,** 77–79 (2001).
3. Lezec, H. J., Dionne, J. A. & Atwater, H. A. Negative refraction at visible frequencies. *Science* **316,** 430–432 (2007).
4. Valentine, J. *et al.* Three-dimensional optical metamaterial with a negative refractive index. *Nature* **455,** 376–379 (2008).
5. Zhang, S. *et al.* Experimental demonstration of near-infrared negative-index metamaterials. *Phys. Rev. Lett.* **95,** 137404 (2005).
6. Shalaev, V. M. *et al.* Negative index of refraction in optical metamaterials. *Opt. Lett.* **30,** 3356–3358 (2005).
7. Dolling, G., Enkrich, C., Wegener, M., Soukoulis, C. M. & Linden, S. Simultaneous negative phase and group velocity of light in a metamaterial. *Science* **312,** 892–894 (2006).
8. Soukoulis, C. M., Linden, S. & Wegener, M. Negative refractive index at optical wavelengths. *Science* **315,** 47–49 (2007).

9. Pendry, J. B. Negative refraction makes a perfect lens. *Phys. Rev. Lett.* **85,** 3966–3969 (2000).
10. Fang, N., Lee, H., Sun, C. & Zhang, X. Sub-diffraction-limited optical imaging with a silver superlens. *Science* **308,** 534–537 (2005).
11. Taubner, T., Korobkin, D., Urzhumov, Y., Shvets, G. & Hillenbrand, R. Near-field microscopy through a SiC superlens. *Science* **313,** 1595–1595 (2006).
12. Maslovski, S. & Tretyakov, S. Phase conjugation and perfect lensing. *J. Appl. Phys.* **94,** 4241–4243 (2003).
13. Pendry, J. B. Time reversal and negative refraction. *Science* **322,** 71–73 (2008).
14. Allen, C. A., Leong, K. M. K. H. & Itoh, T. A negative reflective/refractive meta-interface using a bi-directional phase-conjugating array. *IEEE Int. Microw. Theory Tech. Symp. Dig.* **3,** 1875–1878 (2003).
15. Fusco, V. F. *et al.* Active phase conjugating lens with sub-wavelength resolution capability. *IEEE Trans. Antennas Propag.* **58,** 798–808 (2010).
16. Katko, A. R. *et al.* Phase conjugation and negative refraction using nonlinar active metamaterials. *Phys. Rev. Lett.* **105,** 123905 (2010).
17. Bloembergen, N. & Pershan, P. S. Light waves at the boundary of nonlinear media. *Phys. Rev.* **128,** 606–622 (1962).
18. Boyd, R. W. *et al.* (eds) *Nonlinear Optics* (Academic, 2003).
19. Bartal, G., Manela, O. & Segev, M. Spatial four wave mixing in nonlinear periodic structures. *Phys. Rev. Lett.* **97,** 073906 (2006).
20. Smith, D. D. *et al. z*-scan measurement of the nonlinear absorption of a thin gold film. *J. Appl. Phys.* **86,** 6200–6205 (1999).
21. Klein, M. W., Enkrich, C., Wegener, M. & Linden, S. Second-harmonic generation from magnetic metamaterials. *Science* **313,** 502–504 (2006).
22. Renger, J., Quidant, R., van Hulst, N. & Novotny, L. Surface-enhanced nonlinear four-wave mixing. *Phys. Rev. Lett.* **104,** 046803 (2010).
23. Su, K. H., Wei, Q. H. & Zhang, X. Tunable and augmented plasmon resonances of Au/SiO_2/Au nanodisks. *Appl. Phys. Lett.* **88,** 063118 (2006).
24. Palomba, S. & Novotny, L. Nonlinear excitation of surface plasmon polaritons by four-wave mixing. *Phys. Rev. Lett.* **101,** 056802 (2008).
25. Maier, S. A. *et al.* Local detection of electromagnetic energy transport below the diffraction limit in metal nanoparticle plasmon waveguides. *Nature Mater.* **2,** 229–232 (2003).

Acknowledgements

The authors acknowledge funding support from the US Army Research Office (MURI W911NF-09-1-0539).

Author contributions

S.P. conducted the measurements. S.P. and S.Z. performed numerical simulations. Y.P. fabricated the samples. S.P., G.B., X.Y., S.Z. and X.Z. analysed the experimental data and wrote the manuscript. X.Z., X.Y. and G.B. guided the research. All authors contributed to discussions.

Additional information

The authors declare no competing financial interests. Reprints and permissions information is available online at http://www.nature.com/reprints. Correspondence and requests for materials should be addressed to X.Z.